Chapter 6

Failure Analysis

This section is devoted to the failure analysis of the models analyzed in the previous chapters. In section 6.2 various criteria accounted for the failure initiation are described. The Crack band method for the progressive failure analysis in a mesh objective way is analyzed in section 6.3. Numerical results are presented in section 6.4.

6.1   Introduction

Composite materials are increasingly being used in many engineering fields since their excellent specific properties are advantageous for the design of many structures, such as aircraft or cars. The characterization of failure mechanisms is a crucial issue to fully exploit composite material capabilities. As shown in Figure 6.1, various phenomena as matrix micro cracking, delamination between plies, debonding between fiber and matrix material (pull-out) can lead to the failure of composite structures. Performing failure analysis requires enhanced structural analysis capabilities to detect accurate stress/strain fields in the matrix, fibers, layers and interfaces of composite structures. Composites have very different and more complex failure modes from those of traditional metallic structures. A wide number of criteria exist to predict the occurrence of failure in fiber-reinforced composite materials. They can be classified depending on the stress/strain components that are considered. A brief overview of the most important two-dimensional failure criteria for anisotropic materials is given in [61], while [62] considers a 3D stress/strain states. The World Wide Failure Exercise (WWFE) provided a comprehensive assessment of the methods for predicting the failure initiation in fiber-reiforced composites. From the WWFE, Puck failure criterion [63] has emerged as the most effective. Inspired by Puck's assumptions, NASA Langley Research Centre has formulated some improved criteria for the 2D- and the 3D-state of stress, LaRC03 [64] and LaRC04 [65] respectively. These developments are aimed at limiting the number of experimental tests needed in the design of composite structures. Once the failure initiation is identified, a progressive failure analysis has to be performed to identify the damage propagation. The failure analysis is the main tool to properly understand the mechanical behaviour of composite structure, improve the design and prevent catastrophic failures.
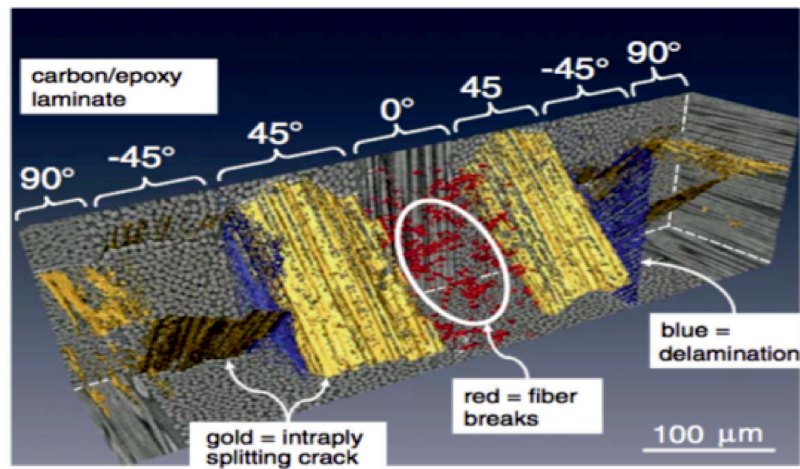
Fig. 3.5 X-ray computed tomography image of damage in a quasi-isotropic carbon/epoxy laminate (Ian Sinclair, University of Southampton, UK, 2007) (Reproduced by kind permission)

Figure 6.1.   Failure phenomena [Camañho, Dávila, Pinho and Remmers: Mechanical response of Composites].

6.2   Failure initiation analysis

Based on the stress and strain distributions different kind of failure criteria can be taken into account. Material strength parameters need to be known to perform failure analysis.
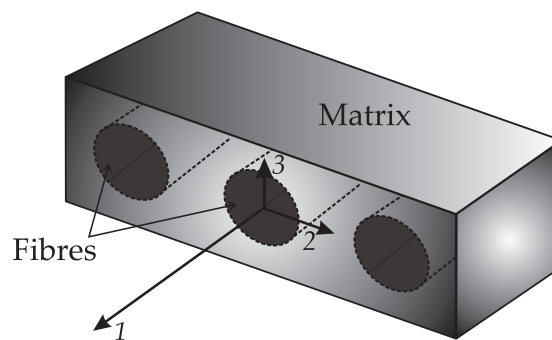

Figure 6.2.   Reference system for the failure analysis.

Since tests are performed in the principal material directions to characterize these parameters, all the assessments proposed in this chapter refers to the system (1,2,3) shown in Figure 6.2 where the fibers are parallel to the 1-axis. A number of failure criteria have been formulated in the last decades in order to predict failure loads under arbitrary stress states. The basic idea of these criteria is to define a "failure envelope" within which preexistent damages don't turn into failure. Where "Damage", is regarded as a defect that, depending on the loading configuration, can occur in the matrix (microcracking) or in the

fibers (kinking, fiber microbuckling). Damage propagation may lead to a complete "Failure" where the structural integrity is lost. According with this idea, a failure criterion can be described as a formulation used to identify the stress vector that lead to a failure mode. The criterion conditions can be mathematically expressed as:

$$F(\sigma_i, X_i) = 1 \qquad i = 1,...,k \qquad (6.1)$$

where σ_i is the ith component of the stress vector, X_i is a strength parameter that depends on the material and k is the number of fracture conditions imposed by the criterion. Since the strength parameters in tension or compression can be different, k depends on the stress state. X_i can be measured experimentally for uniaxial or pure shear states. It has to be noted that, strengths are always defined as positive values. Criteria can be classified into two main groups depending on the stress interactions taken into account. Those that neglect the interactions between the stress components are the simplest. One inequality for each of the three in-plane stress (or strain) components is proposed, the maximum strain and maximum stress criteria [16] belong to this group. When interactions are taken into account, for defining the failure envelope can be either used a single inequality, as in Hoffman [66], Tsai-Wu [67, 68] and Tsai-Hill [69, 70], or a set of interactive and non-interactive conditions as in the Hashin [71, 72] and Puck [73, 63] criteria. A failure parameter referred as "Failure Index", FI, is identified for each criterion. The failure initiation is determined when FI exceeds the unitary value. In the next sections, some well known criteria are shown. Since the multiscale approaches proposed in this thesis no assumptions of plane stress have been made, the 3D criteria are taken into account and implemented in FORTRAN environment within the CUF.

6.2.1   3D Maximum Stress Criterion

The Maximum Stress criterion (MS) does not consider any interaction between different stress components. It is based on the concept that the failure occurs when a stress component exceeds the correspondent critical value in at least one direction. The conditions

for the MS of an anisotropic material can be summed up as follows:

$$\sigma_{11} \geq 0 \;\Rightarrow\; \sigma_{11} \geq X_T$$
$$\text{or}$$
$$\sigma_{11} < 0 \;\Rightarrow\; \sigma_{11} \leq X_C$$

$$\sigma_{22} \geq 0 \;\Rightarrow\; \sigma_{22} \geq Y_T$$
$$\text{or}$$
$$\sigma_{22} < 0 \;\Rightarrow\; \sigma_{22} \leq Y_C$$

$$\sigma_{33} \geq 0 \;\Rightarrow\; \sigma_{33} \geq Z_T \qquad (6.2)$$
$$\text{or}$$
$$\sigma_{33} < 0 \;\Rightarrow\; \sigma_{22} \leq Z_C$$

$$\tau_{12} \geq S_{12}^L$$
$$\tau_{13} \geq S_{13}^L$$
$$\tau_{23} \geq S_{23}^L$$

where X, Y and Z are respectively the strength parameter in 1-, 2- and 3- directions. X, Y and Z can also be addressed as "Failure Coefficients", FC. For anisotropic materials these parameters depends on the direction and are usually all different from each other while, for isotropic materials just one value has to be identified. Besides, different values can be found for traction or compression loadings; the superscripts "T","C" indicate the corresponding strength values in the axial traction and compression cases. The superscript "L" indicates a strength parameter in a shear direction. Also, for anisotropic materials depending on the shear loading, three different strength values have to be considered, $L_1 = 12$, $L_2 = 13$, $L_3 = 23$. For the Maximum Stress criterion the FI is obtained as follows; failure occurs when the index becomes greater or equal to one.

$$FI = \max \left[\frac{\sigma_{ij}}{FC^{T,C}} \right] \qquad (6.3)$$

6.2.2   3D Maximum Strain Criterion

The Maximum Strain Criterion (MSt) is obtained following the same approach as for maximum stress, but the strain components are taken into account:

$$\varepsilon_{11} \geq 0 \ \Rightarrow \ \varepsilon_{11} \geq \varepsilon_{11}^{T}$$
$$\text{or}$$
$$\varepsilon_{11} < 0 \ \Rightarrow \ \varepsilon_{11} \leq \varepsilon_{C}$$

$$\varepsilon_{22} \geq 0 \ \Rightarrow \ \varepsilon_{22} \geq \varepsilon_{22}^{T}$$
$$\text{or}$$
$$\varepsilon_{22} < 0 \ \Rightarrow \ \varepsilon_{22} \leq \varepsilon_{22}^{C}$$

$$\varepsilon_{33} \geq 0 \ \Rightarrow \ \varepsilon_{33} \geq \varepsilon_{33}^{T} \tag{6.4}$$
$$\text{or}$$
$$\varepsilon_{33} < 0 \ \Rightarrow \ \varepsilon_{33} \leq \varepsilon_{33}^{C}$$

$$\gamma_{12} \geq \gamma_{12}^{L}$$
$$\gamma_{13} \geq \gamma_{13}^{L}$$
$$\gamma_{23} \geq \gamma_{23}^{L}$$

For the MSt the FC can be ε or γ respectively for the axial and shear direction. As for the maximum stress criterion the superscripts "T","C","L" indicate the corresponding strength parameters respectively in the axial traction/compression and shear directions. Since the stress/strain relation is described by the Hook's law, the two criteria are equivalents. The FI is obtained as:

$$FI = \max\left[\frac{\varepsilon_{ij}}{FC^{T,C}}\right] \tag{6.5}$$

6.2.3   3D Tsai-Hill Criterion

The Tsai-Hill (TH) is an interactive quadratic criterion. It represents the extension to composite materials of the Von Mises criterion used to analyze metals. This criterion was formulated by referring to distortion energy. It is known that total strain energy in a body is composed of two parts: the distortion energy which cause change in shape and the second, a dilation energy which causes the change in size or volume. In the Von Mises criterion it is assumed that the material fails when the maximum distortion energy of the body exceeds the distortion energy corresponding to yielding in tension. Hill extended the von Mises distortion energy criterion of isotropic materials to anisotropic materials, later Tsai extended this criterion for anisotropic materials to unidirectional laminae.

$$\left(\frac{\sigma_{11}}{X}\right)^2 + \left(\frac{\sigma_{22}}{X}\right)^2 + \left(\frac{\sigma_{33}}{X}\right)^2 - A\sigma_{11}\sigma_{22} - B\sigma_{11}\sigma_{33} - C\sigma_{22}\sigma_{33}+$$
$$\left(\frac{\sigma_{23}}{S_{23}}\right)^2 + \left(\frac{\sigma_{31}}{S_{13}}\right)^2 + \left(\frac{\sigma_{12}}{S_{12}}\right)^2 \geq 1 \tag{6.6}$$

$$A = \frac{1}{X^2} + \frac{1}{Y^2} - \frac{1}{Z^2}$$
$$B = \frac{1}{X^2} - \frac{1}{Y^2} + \frac{1}{Z^2} \tag{6.7}$$
$$C = \frac{1}{Y^2} + \frac{1}{Z^2} - \frac{1}{X^2}$$

The FCs, A, B and C are a combination of the strength parameters in 1-,2- and 3- directions. For sake of simplicity in the presented notation the superscripts T,C are not reported. The equation 6.6 shows the failure envelope according to the TH where the left hand side of the equation represent the related FI. This criterion, being based on von Mises hypothesis, is more suitable for ductile materials.

6.2.4 3D Tsai-Wu Criterion

The Tsai-Wu (TW) is a quadratic interaction tensor polynomial failure criterion. It is based on the theoretical assumption that exists a failure surface in the stress-space in the following scalar form:

$$f(\sigma_k) = F_i \sigma_i + F_{ij} \sigma_i \sigma_j = 1 \qquad i,j,k + 1,...,6 \tag{6.8}$$

where F_i and F_{ij} are strength tensors respectively of second and fourth orders. In this criterion the linear part, σ_i, takes into account the difference between the sign of the stress that induces the failure while the quadratic term, $\sigma_i \sigma_j$, defines and ellipsoid in the stress space. By expanding the Equation 6.8 the criterion become:

$$A_{11}\sigma_{11}^2 + A_{22}\sigma_{22}^2 + A_{33}\sigma_{33}^2 + B_1\sigma_{11} + B_2\sigma_{22} + B_3\sigma_{33} + 2A_{12}\sigma_{11}\sigma_{22} +$$
$$2A_{13}\sigma_{11}\sigma_{33} + 2A_{23}\sigma_{22}\sigma_{33} + A_{66}\tau_{12}^2 + A_{55}\tau_{13}^2 + A_{44}\tau_{23}^2 \geq 1 \tag{6.9}$$

where the coefficients, A_{11},...,A_{66} reported in Equation 6.10 can be obtained as in [74].

$$A_{11} = \frac{1}{X^T X^C}$$
$$A_{22} = \frac{1}{Y^T Y^C}$$
$$A_{33} = \frac{1}{Z^T Z^C}$$
$$B_1 = \frac{1}{X^T} - \frac{1}{X^C}$$
$$B_2 = \frac{1}{Y^T} - \frac{1}{Y^C}$$
$$B_3 = \frac{1}{Z^T} - \frac{1}{Z^C} \tag{6.10}$$
$$A_{12} = \frac{1}{2\sqrt{X^T X^C Y^T Y^C}}$$
$$A_{13} = \frac{1}{2\sqrt{X^T X^C Z^T Z^C}}$$
$$A_{23} = \frac{1}{2\sqrt{Y^T Y^C Z^T Z^C}}$$
$$A_{44} = A_{55} = A_{66} = \frac{1}{S^L S^L}$$

6.2.5 3D Hashin Criterion

The Hashin criterion proposes a combination of four interactive and non-interactive conditions in order to distinguish between matrix and fiber failure caused by tension or compression. It is an interactive criterion; fiber inequalities are shown in Equation 6.11, while in Equation 6.12 the inequalities for the matrix are reported. This criterion involves four failure modes in 2D, the Equation 6.13 refers to the interlaminar failure mode that is represented by the maximum stress criterion in the lamina out-of-plane direction.

$$Fiber : \begin{cases} (\frac{\sigma_{22}}{Y_T})^2 + \frac{\sigma_{12}^2 + \sigma_{23}^2}{S_{12}^2} & \text{if } \sigma_{22} >= 0 \\ (\frac{\sigma_{22}}{Y_C})^2 & \text{if } \sigma_{22} < 0 \end{cases} \tag{6.11}$$

$$Matrix : \begin{cases} \frac{(\sigma_{11} + \sigma_{33})^2}{X_T^2} + \frac{\sigma_{13}^2 - \sigma_{11}\sigma_{33}}{S_{13}^2} + \frac{\sigma_{12}^2 + \sigma_{23}^2}{S_{12}^2} & \text{if } \sigma_{11} + \sigma_{33} >= 0 \\ \left[\frac{X_C}{2S_{13}} - 1\right]\left(\frac{\sigma_{11} + \sigma_{33}}{X_C}\right) + \frac{(\sigma_{11} + \sigma_{33})^2}{4S_{13}^2} + \frac{\sigma_{13}^2 - \sigma_{11}\sigma_{33}}{S_{13}^2} + \frac{\sigma_{12}^2 + \sigma_{23}^2}{S_{12}^2} & \text{if } \sigma_{11} + \sigma_{33} < 0 \end{cases} \tag{6.12}$$

$$Interlaminar : \begin{cases} (\frac{\sigma_{33}}{Z_T})^2 & \text{if } \sigma_{33} >= 0 \\ (\frac{\sigma_{33}}{Z_C})^2 & \text{if } \sigma_{33} < 0 \end{cases} \tag{6.13}$$

6.2.6 Puck and LaRC04 Criteria

Most failure conditions previously described are mainly based on mathematical interpolation functions. Puck's criterion, is based on a experimental work that led to formulate some fracture hypotheses. It can distinguish between fiber fracture (FF) and inter-fibre fracture (IFF). For sake of brevity the mathematical formulation is not reported here but it can be found in the [75]. Both 2D and 3D formulations are available. Based on the Puck's hypotheses the LaRC03 and LaRC04 have been formulated at Langley Research Center in relation to the WWFE. A detailed description of the LaRC criteria can be found in [64] and [65]. The Larc03 criterion, based on the 2D state of stress, can predict matrix and fiber failure accurately. A specific criterion for the fiber kinking is obtained by calculating the fiber misalignment and applying the matrix failure criterion in the misaligned coordinate frame. Fracture mechanics models for microcracks are used to develop a criterion for matrix failure in tension and to calculate the associated in-situ strengths. The Larc04 criterion consists of six mathematical expressions. It is based on physical models for each failure mode and takes into account the non-linear matrix shear behaviour. The model for matrix compressive failure is based on the Mohr-Coulomb criterion and it also predicts the fracture angle. Fiber kinking is triggered by an initial fiber misalignment angle and by the rotation of the fibers during compressive loading. The plane of fiber kinking is also predicted by the model.

6.3 Progressive Failure Analysis

Once the stress distribution is obtained with good accuracy and the failure initiation criterion is satisfied, a degradation scheme has to be introduced to model the crack propagation and performing the progressive failure analysis in the model. Among many available techniques for the progressive failure analysis of composite structures, cohesive zone model (CZM) elements have been extensively used [76],[77]. Nevertheless, this technique requires to place the cohesive elements along the potential failure path that is not usually known a priori. The elements are activated when the failure criterion is satisfied and the decohesive behavior is introduced. A wide number of elements is needed to perform the analysis, and since reducing the computational effort of the analysis is still a challenging task in modeling composites, it is important to underline that the DOFs involved in this approach can be prohibitively hight. In this work, the fracture is modeled through the crack band method as formulated by Bazant and Oh [78] for concrete. This approach is meant to capture the bahavior of a region in which many microcraks coalesce in a larger crack also referred as crack band. Implementing this approach in a FE framework also guarantees mesh independent results that arise because the failure localizes and all of the energy is dissipated over a volume that is a function of the FE discretization. Within the crack band model, microcracks are considered spread over the finite elements and when the post-peak softening regime is reached, the dissipated energy becomes function of a characteristic length, l_c. Since the effect of microcraks in the matrix wants to be analyzed and in a monolithic material cracks orient such that the crack tips are always subjected to mode I, just the opening mode depicted in Figure 6.3, has herein been considered. The crack band is assumed to be oriented depending on the direction of the maximum


Mode I
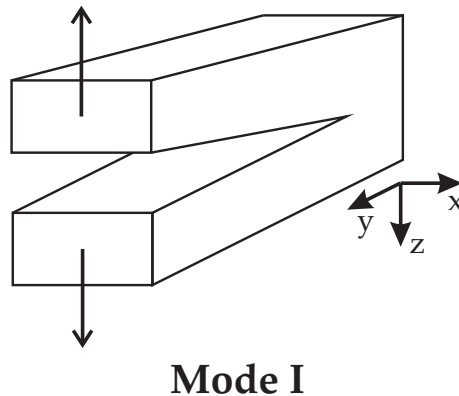
Figure 6.3. Stress-strain diagram for the fracture process.

principal stress. The maximum strain criterion is herein used to determine the failure initiation. As shown in Figure 6.4 before to reach the peak in the stress-strain curve, the meterial is assumed to have an linear elastic behavior. After the peak in the stress-strain curve the traction-separation law domain is entered and the continuum mechanics is not valid anymore. A progressive strain-softening (the decreasing of the stress when the strain increases) is experienced in the model. In the crack band theory, when the characteristic
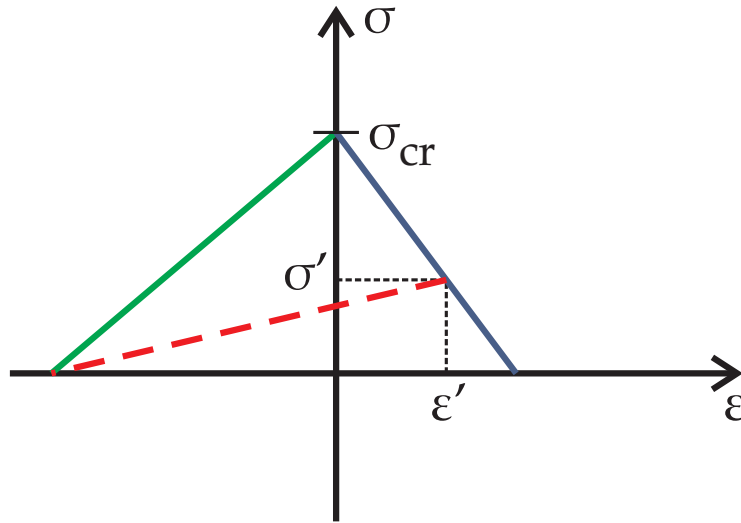
Figure 6.4. Stress-strain diagram for the fracture process.

lenght l_c is introduced, the graph depicted in Figure 6.4 can be obtained in terms of the G_{IC} as shown in Figure 6.3 where, the fracture toughness G_{IC}, is the fracture energy consumed in the formation and opening of all the microcracks smeared in the element also addressed as critical "energy release rate".
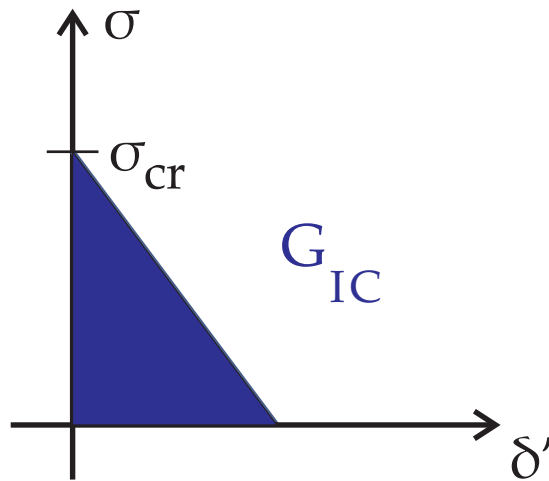

Figure 6.5. $\sigma - \delta'$ diagram for the fracture process.

$$\delta' = (\varepsilon' - \varepsilon_{cr})l_c \tag{6.14}$$

The displacement δ' is defined in equation 6.14.

$$\sigma' = \sigma_{cr}\left(\frac{1 - \delta'\sigma_{cr}}{2G_{IC}}\right) \tag{6.15}$$

The secant tangent stiffness is used to avoid the illness caused by the negative tangent slope. The degraded Young modulus is then given by:

$$E' = \frac{\sigma'}{\varepsilon'} \tag{6.16}$$

The described procedure can be summed up as shown in the algorithm reported in Figure 6.3. Where the average stress over the cell is defined as:
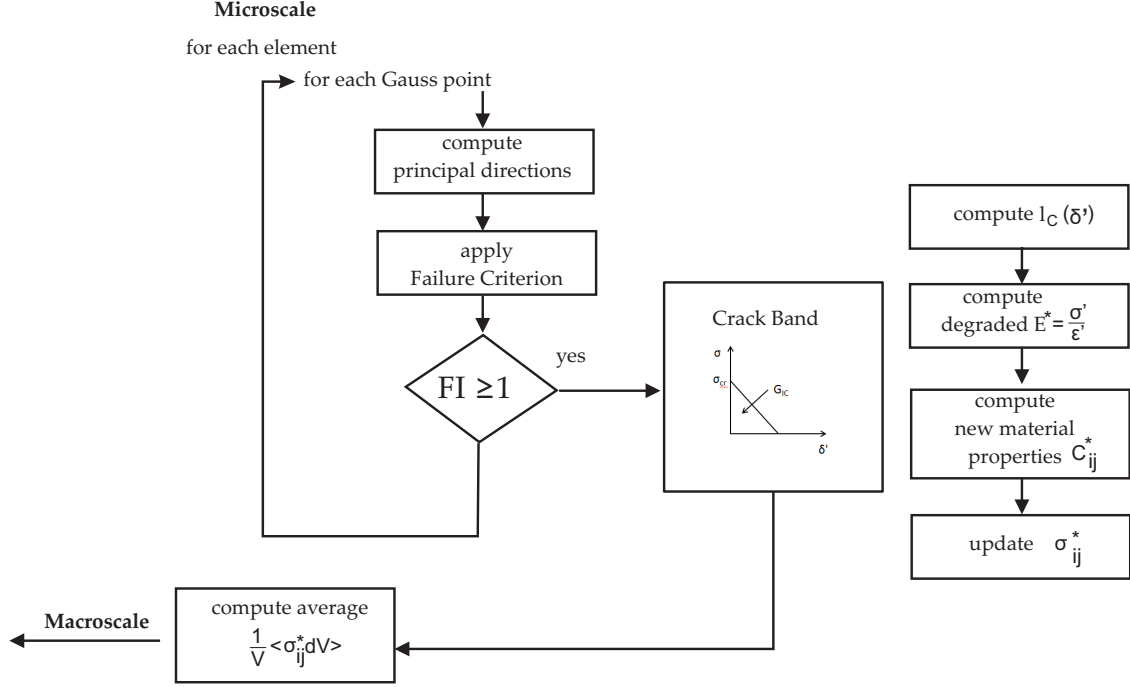

Figure 6.6.   Algorithm used to implement the Crack-Band method in the 1D CUF formulation.

$$\sigma'_{av} = \frac{1}{V} \int_{V_i} \sigma'_{ij} dV_i \tag{6.17}$$

In the framework of the 1D CUF the characteristic length has been computed defining a 3D fictitious element as shown in chapter 4 starting from the LE nodes on the cross-section and the nodes in the beam direction in the (x,y,z) physical frame. The volume of the fictitious element is also used to compute the average stress in the the RUC. In the implemented algorithm, for each Gauss Point of the 3D fictitious element, the maximum strain criterion is applied to determine the failure initiation. When the criterion is satisfied, the characteristic length is evaluated as distance between the intersection of the points along the line perpendicular to the maximum principal direction that goes from the center and the external surface of the element. The l_c is depicted in Figure 6.3 for a fictitious element obtained from 1 L9+1 B3 mesh; for sake of simplicity, a 2D l_c description has also been provided. Since the tangent slope in the stress-strain law, E, becomes negative

MICROSCALE
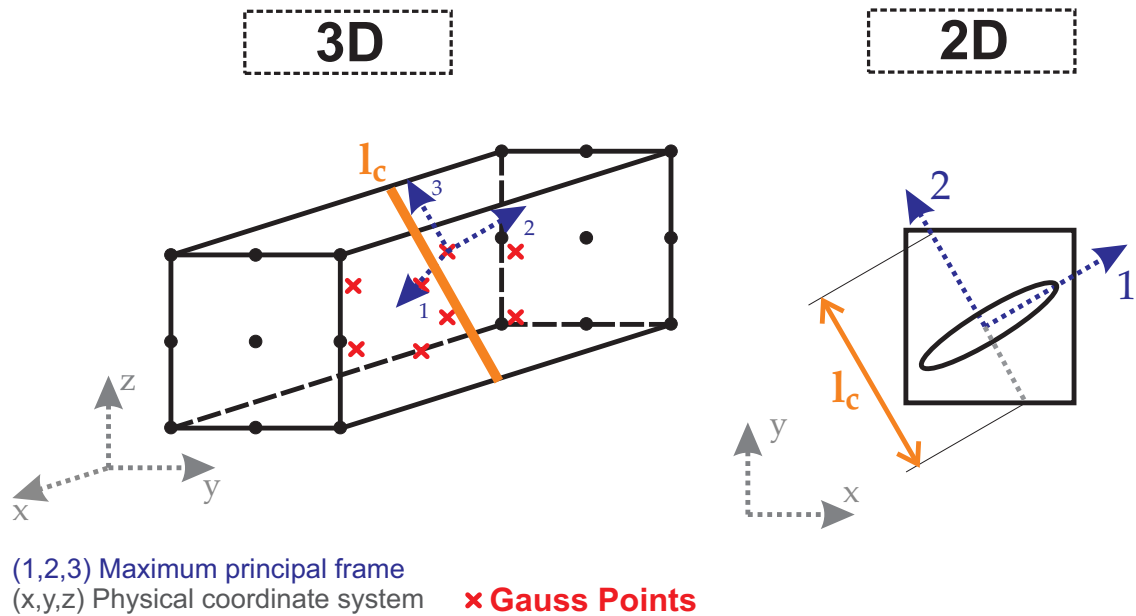
Figure 6.7.   Evaluation of the characteristic lenght, l_c.

when failure happens (Figure 6.4), the characteristic length has to respect the following mathematical condition:

$$l_c < \frac{2G_{IC}E}{\sigma_{cr}^2} \tag{6.18}$$

Results provided in section 6.4 show that, using the crack band method, the mesh objectivity is actually guaranteed. This accomplishment and the use of 1D elements, make the analysis reliable and computationally convenient. Furthermore since the discontinuity is embedded in the finite element formulation itself, there is no need for the crack path to be known ahead of time in the simulation. More details about the crack band formulation can be found in [78].

6.4 Numerical Results

Many numerical examples are discussed in this section. Preliminary assessments are carried out on simple homogeneous structures in order to validate the present formulation for determining the failure initiation. Then, a fiber-matrix cell and a double cell are analyzed; the evaluation of the failure index distributions according to different criteria is shown. Further assessments are provided for laminates where fiber/matrix cells are included in different part of the models. Comparisons with results from plate and solid models are provided. For the progressive failure analysis, first a square homogeneous model is used to prove the mesh objectivity. Then, results for the single fiber and the hexagonally packed RUCs are provided.

6.4.1 Preliminary assessments

A thin plate was first considered in order to provide preliminary results in terms of failure indexes. The plate cross-section is shown in Fig. 6.8. The length of the the plate, L, equal to 0.1 m, L/b equal to 10 and L/h equal to 100. The plate was clamped at one end and a vertical point load was applied to the center point of the free tip cross-section, F_z equal to -5.0 N. An orthotropic material was used and its properties are given in Table 6.1. Results were evaluated in terms of failure indexes as shown in Tables 6.2 and 6.3. Two beam models based on LE expansions were exploited and a plate model from MSC Nastran was used for comparison purposes. An excellent agreement was found between beam and plate results.
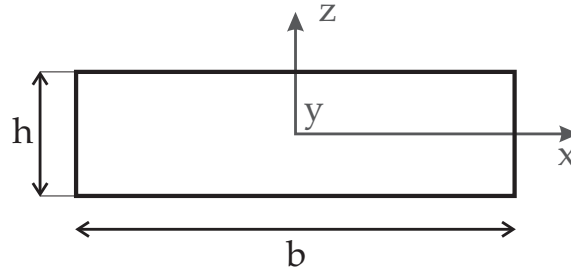

Figure 6.8.   Plate cross-section.

Elastic Properties		Stress Limits		Strain Limits	
E_1	127.6 GPa	σ_{11T}	1.730 GPa	ϵ_{11T}	0.0138
E_2,E_3	11.3 GPa	σ_{11C}	1.045 GPa	ϵ_{11C}	0.01175
G_{12},G_{13}	6.0 GPa	$\sigma_{22T}, \sigma_{33T}$	66.5 MPa	$\epsilon_{22T}, \epsilon_{33T}$	0.00436
G_{23}	1.8 GPa	$\sigma_{22C}, \sigma_{33C}$	255.0 MPa	$\epsilon_{22C}, \epsilon_{33C}$	0.002
ν_{12},ν_{13}	0.3	$\sigma_{12}, \sigma_{13}, \sigma_{23}$	95.1 MPa	$\epsilon_{12}, \epsilon_{13}, \epsilon_{23}$	0.002
ν_{23}	0.36				

Table 6.1.   Orthotropic material properties.

	1 L9	3 × 3 L9	Plate
$z = +h/4$			
Max Stress	0.077	0.077	0.077
Max Strain	0.191	0.121	0.121
Tsai-Wu	−0.033	−0.031	−0.032
$z = -h/4$			
Max Stress	0.128	0.128	0.128
Max Strain	0.089	0.091	0.089
Tsai-Wu	0.052	0.049	0.052

Table 6.2.   Failure indexes at $x = b/2$, $y = L/10$, thin plate.

	1 L9	3 × 3 L9	Plate
$z = +h/4$			
Max Stress	0.080	0.079	0.077
Max Strain	0.200	0.191	0.146
Tsai-Wu	−0.033	−0.040	−0.038
$z = -h/4$			
Max Stress	0.132	0.131	0.130
Max Strain	0.092	0.091	0.091
Tsai-Wu	0.053	0.060	0.060

Table 6.3.   Failure indexes at $x = 0$, $y = L/10$, thin plate.

A compact isotropic beam was then considered as further preliminary assessment in order to compare the results from 1D CUF with those from a solid finite element model. A square cross-section was considered with $h = 0.1$ mm and $L/h = 10$. More details about this case study can be found in chapter where the three different L9 distributions and results in terms of stress distribution were also shown. Materials are isotropic, the mechanical and failure properties are given in chapter 3 (Table 6.5). The beam was clamped and a vertical force was applied at the center point of the free-tip cross-section, $F_z = -0.1$ N. In Table 6.4 in terms failure indexes at point A $[0, L/2, h/2]$ and point C

	Point A			
	1 L9	4 L9	16 L9	SOLID
Max Stress	0.1734	0.1734	0.1731	0.17341
Max Strain	0.1704	0.1704	0.1701	0.17037
	Point C			
	1 L9	4 L9	16 L9	SOLID
Max Stress	0.1314	0.2077	0.1955	0.18184
Max Strain	0.1274	0.2013	0.1894	0.17619

Table 6.4.   Failure indexes for the isotropic beam at $L/2$.

$[b/2, L/2, 0]$. For this preliminary assessment, it can be stated that there is an excellent agreement between 1D CUF and the solid model and, in particular, the refinement of the L9 distribution improves the shear stress and the failure index detection significantly.

6.4.2 Fiber/Matrix Cells

A single and a double matrix cell are taken into account in the present section. Geometry and loading case configurations are shown in chapter 3.3.2 where the 12 L9 and 8 L6 elements mesh is depicted and results in terms of stress distribution were also presented. Material properties and failure coefficients for stress and strain are listed in Table 6.5. Tables 6.6 and 6.7 refer respectively to the single CW fiber/matrix cell for a bending

	Fiber	Matrix
Material Properties		
E [GPa]	250.6	3.252
ν [-]	0.2456	0.355
Failure Coefficients		
Maximum Stress [MPa]		
X^T	3398.1	66.5
X^C	2052.6	255
S^L	186.8	74
Maximum Strain [-]		
ε^T	0.0138	0.00436
ε^C	0.01175	0.002
γ^L	0.004	0.0016

Table 6.5. Material properties and failure coefficients.

loading, $F_z = -0.1$ N, applied at the beam free tip, center of the cell.
Figure 6.9 shows the FI distribution for the Solid, TE and LE single fiber models at $y = 0$ where the beam is clamped. For the double cell, whose geometry is described in section 3.4, the failure initiation analysis has been performed; two vertical point loads $F_z = -0.07$ N are applied at the center of each cell. Tables 6.8 and 6.9 show the FI at points E,E',F and F' while the FI distribution at the clamped cross-section for the Solid, TE (N=8) and LE models. The point coordinates are shown in Figure 6.10.

6.4.3 Laminates

A cantilever laminated [0/90/0] beam failure analysis is herein proposed. The height (h_i) of each ply and the width (b) are equal to 0.2 mm and 0.8 mm, respectively. A fiber/matrix cell is modeled as having a geometry of the previous analyzed cells as shown in Figure 6.4.3. The structure is clamped at $y = 0$ and the FI for two different loading configurations are proposed. First, a bending force is locally applied on the center of the second lamina as shown in Figure 4.16, $F = 5$ N. Then, four torsion forces, F = 1 N, have been applied. More details about the model are given in chapter 4. Results are provided in Figure 6.12

Failure Index - Maximum Stress				
Model	Point B	Point D	Point B'	Point D'
	at y = L/2		at y = 0	
Classical Beam Model				
EBBT	0.28	0.00	0.56	0.00
TBM	0.28	0.11	0.56	0.11
TE				
N=1	0.28	0.11	0.56	0.11
N=2	0.28	0.13	2.66	1.10
N=3	0.28	0.13	2.58	1.08
N=4	0.28	0.13	2.83	1.28
N=5	0.28	0.13	2.81	1.28
N=6	0.28	0.13	2.81	1.26
N=7	0.28	0.13	2.80	1.26
N=8	0.28	0.13	2.77	1.24
LE				
	0.28	0.14	1.44	0.95
SOLID				
	0.28	0.13	1.30	0.96

Table 6.6.   Failure Index for the single cell CW model Point B,D and Point B',D': Maximum Stress criterion.

for the bending load configuration while in Figure 6.12 the fiber/matrix behavior in the torsion case study is analyzed.   Following a comparison between the TE,CW and Solid results, the subsequent remarks can be made:

1. the CW approach provides an accurate description of the cell stress/strain fields and facilitates the identification of the area where the critical condition occurs;

2. the convergence of the Failure Index of the 1D-models to those of Solid models depends on the axial and shear stress convergence. The clamped cross-section is a critical part of the model, however its behavior is described well by LE model. The TE model requires higher orders to ensure comparable results to the Solid model;

3. since a refined description of the stress and strain states are provided in the subdomain where the cell is included, it is possible to apply failure criteria directly on the components.

4. the LE models are able to describe the cell behavior with the same accuracy as the Solid model; moreover the present CW approach leads to a considerable reduction in computational costs.

	Failure Index - Maximum Strain			
Model	Point B	Point D	Point B'	Point D'
	at y = L/2		at y = 0	
	Classical Beam Model			
EBBT	0.28	0.00	0.55	0.00
TBM	0.28	0.05	0.55	0.05
	TE			
N=1	0.28	0.05	0.55	0.05
N=2	0.28	0.06	1.23	0.51
N=3	0.28	0.06	1.20	0.50
N=4	0.28	0.06	1.31	0.60
N=5	0.28	0.06	1.31	0.60
N=6	0.28	0.06	1.31	0.59
N=7	0.28	0.06	1.30	0.58
N=8	0.28	0.06	1.29	0.57
	LE			
	0.28	0.06	0.67	0.44
	SOLID			
	0.28	0.06	0.60	0.44

Table 6.7. Failure Index for the single cell CW model: Maximum Strain criterion.

6.4.4 Mesh objectivity

To prove the mesh objective of the crack band approach a preliminary study has been conducted in this section. Three different meshes have been used to model a square and homogeneous cell; its geometry is shown in Figure 6.4.4. Dimensions and material properties are given in Table 6.10 and 6.4.4. The post-peak response for the three different meshes have been analyzed. Respectively Mesh 1,2 and 3 are built using 9, 25 and 45 L9 elements on the cross section and 1 B3 element along the beam axis. Figure 6.15 shows the discretization of the three cross-sections; the corresponding DOFs are shown in Table 6.11. Since the RUC is homogeneous, the failure if forced to start in the center of the cell where a lower $\sigma_{cr} = 27.5$ MPa was used as threshold to activate the criterion. The failure is forced to propagate within the elements in the thickness, t, where $\sigma_{cr} = 29.5$. Results in Figure 6.4.4 show that the mesh density has no effect on the stress-strain curve. Since the approach is path independent the first mesh (9 L9) appears to be the best choice to perform the analysis. Then, the single fiber RUC described in the previous chapters has been taken into account. A displacement Δ_x has progressively been applied at $x = x_1$ as shown in Figure 6.4.4 up to the complete failure of the cell. Material properties and failure parameters are listed in Table 6.12. The influence of the fracture toughness on the cell behaviour has also been analyzed; four different G_{IC} have been considered. The corresponding stress-strain curves are shown in Figure 6.4.4 where it can be observed that the curve related to $G_{IC,0}$ shows a plastic behaviour while, when the fracture toughness value decreases to $G_{IC,3}$, a brittle behavior is exhibit.

Failure Index - Maximum Stress				
Model	Point E	Point F	Point E'	Point F'
	at y = L/2		at y = 0	
Classical Beam Model				
EBBT	0.20	0.00	0.39	0.00
TBM	0.20	0.07	0.39	0.07
TE				
N=1	0.20	0.07	0.39	0.07
N=2	0.20	0.12	1.92	1.22
N=3	0.20	0.14	1.86	1.20
N=4	0.19	0.14	2.14	0.94
N=5	0.19	0.13	2.16	0.96
N=6	0.19	0.13	2.01	1.32
N=7	0.19	0.12	1.99	1.32
N=8	0.19	0.12	1.93	1.18
LE				
	0.19	0.12	1.00	0.82
SOLID				
	0.20	0.11	0.90	0.83

Table 6.8.   Failure Index for the double cell CW model: Maximum Stress criterion.

Failure Index - Maximum Strain				
Model	Point E	Point F	Point E'	Point F'
	at y = L/2		at y = 0	
Classical Beam Model				
EBBT	0.19	0.00	0.39	0.00
TBM	0.19	0.03	0.39	0.03
TE				
N=1	0.20	0.07	0.39	0.07
N=2	0.19	0.06	0.89	0.56
N=3	0.19	0.06	0.86	0.56
N=4	0.19	0.06	1.00	0.44
N=5	0.19	0.06	1.00	0.45
N=6	0.19	0.06	0.93	0.61
N=7	0.19	0.06	0.92	0.62
N=8	0.19	0.06	0.89	0.55
LE				
	0.19	0.03	0.46	0.38
SOLID				
	0.19	0.05	0.42	0.38

Table 6.9.   Failure Index for the double cell CW model: Maximum Strain criterion.

	[mm]
t	0.0001
l	0.001
L	0.01

Table 6.10.   Isotropic square cell dimensions

Material Properties	
E	3252 MPa
ν	0.355
G_{IC}	0.0005 N/mm

	DOFs
Mesh 1	441
Mesh 2	1089
Mesh 3	1881

Table 6.11.   DOFs for the isotropic preliminary assessment in the mesh objective failure analysis.

Elastic Properties		Stress Limits		Fracture Taughness	
E_f	250634 MPa	$\sigma_{cr,f}$	3398.1 MPa	$G_{IC,0}$	0.5 N/mm
v_f	0.2456			$G_{IC,1}$	0.05 N/mm
E_m	3252 MPa	$\sigma_{cr,m}$	66.5 MPa	$G_{IC,2}$	0.005 N/mm
v_m	0.355			$G_{IC,3}$	0.0005 N/mm

Table 6.12.   Material properties fort the analysis of the single fiber/matrix RUC

Since the crack-band method is applied at the component scales, it can be included in both the multiscale approaches: the CW and the two-scales techniques respectively presented in chapters 3 and 5. The average stress-strain curve on the cell is provided in Figure 6.19 for $G_{IC,2}$, where the non linearity introduced by the damage is shown. When the traction-separation law is entered a softening in the matrix is induced,then the stress decreases while the strain is increasing. The axial strain ε_{xx} on the cell is shown at different time frames during the evolution of the analysis. The crack path is depicted in 6.19 where in (a) the cell is entering in the traction-separation law since the first elements start to fail; in 6.19 (b) the peak of the stress-strain curve is reached and the matrix properties are degraded. The crack path starts from the top and bottom of the cell as shown in 6.19(c) and 6.20 (d) where the whole crack path is almost defined. At the end of the analysis the matrix is not able to carry any more load and the cell is completely failed, 6.20 (e).

A progressive failure analysis has been also performed for the hexagonally packed cell analyzed in the previous chapters in a mesh objective way. As for the single fiber RUC, a displacement is applied in x-direction leading the cell to a complete failure. The 40 L9 elements mesh stress-strain curve has been compared with a refined 56 L9 elements mesh

depicted in Figure 6.4.4. The stress-strain curve is shown in Figure 6.4.4 for the 40 L9 mesh (1665 DOFs) , mesh 1, and and the 56 L9 (2313 DOFs), mesh 2.
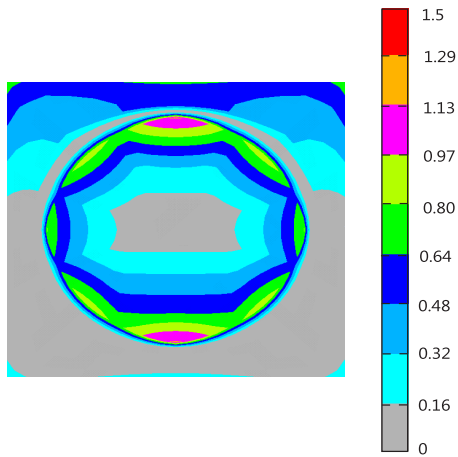
(a) FI Maximum Stress. Solid model.
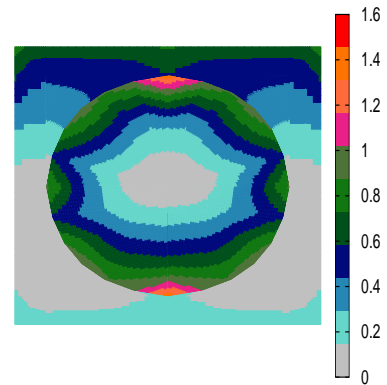
(d) FI Maximum Strain. Solid model.
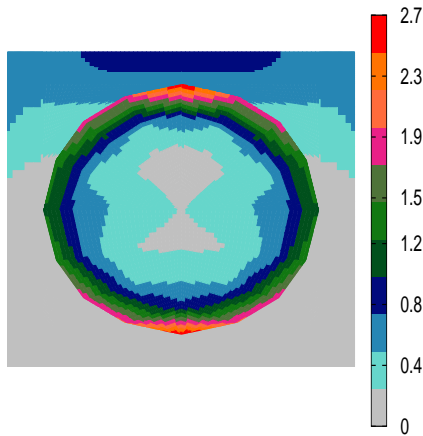
(b) FI Maximum Stress. LE CW model.
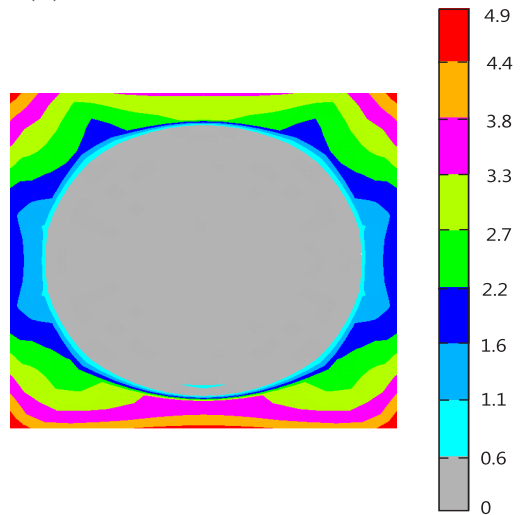
(e) FI Maximum Strain. LE CW model.
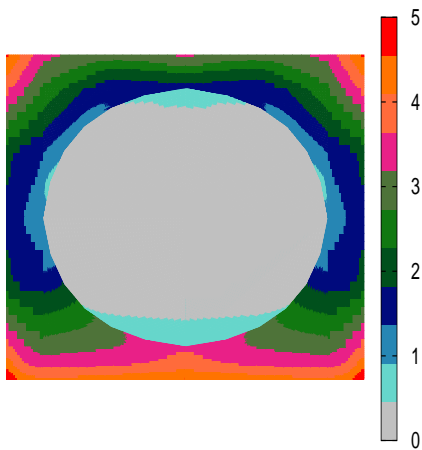
(c) FI Maximum Stress. TE (N=8) CW model.
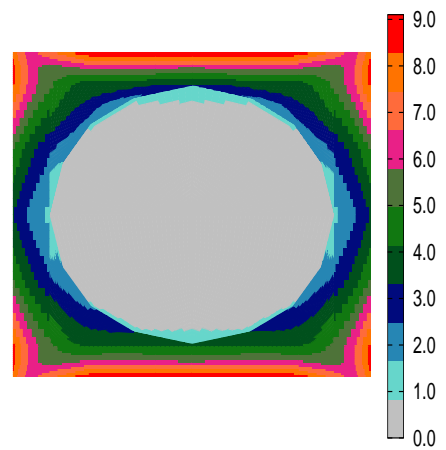
(f) FI Maximum Strain. TE (N=8) CW model.

Figure 6.9. Failure Indexes CW single cell models at $y = 0$.

(a)

(b)

(c)

(d)

(e)

(f)
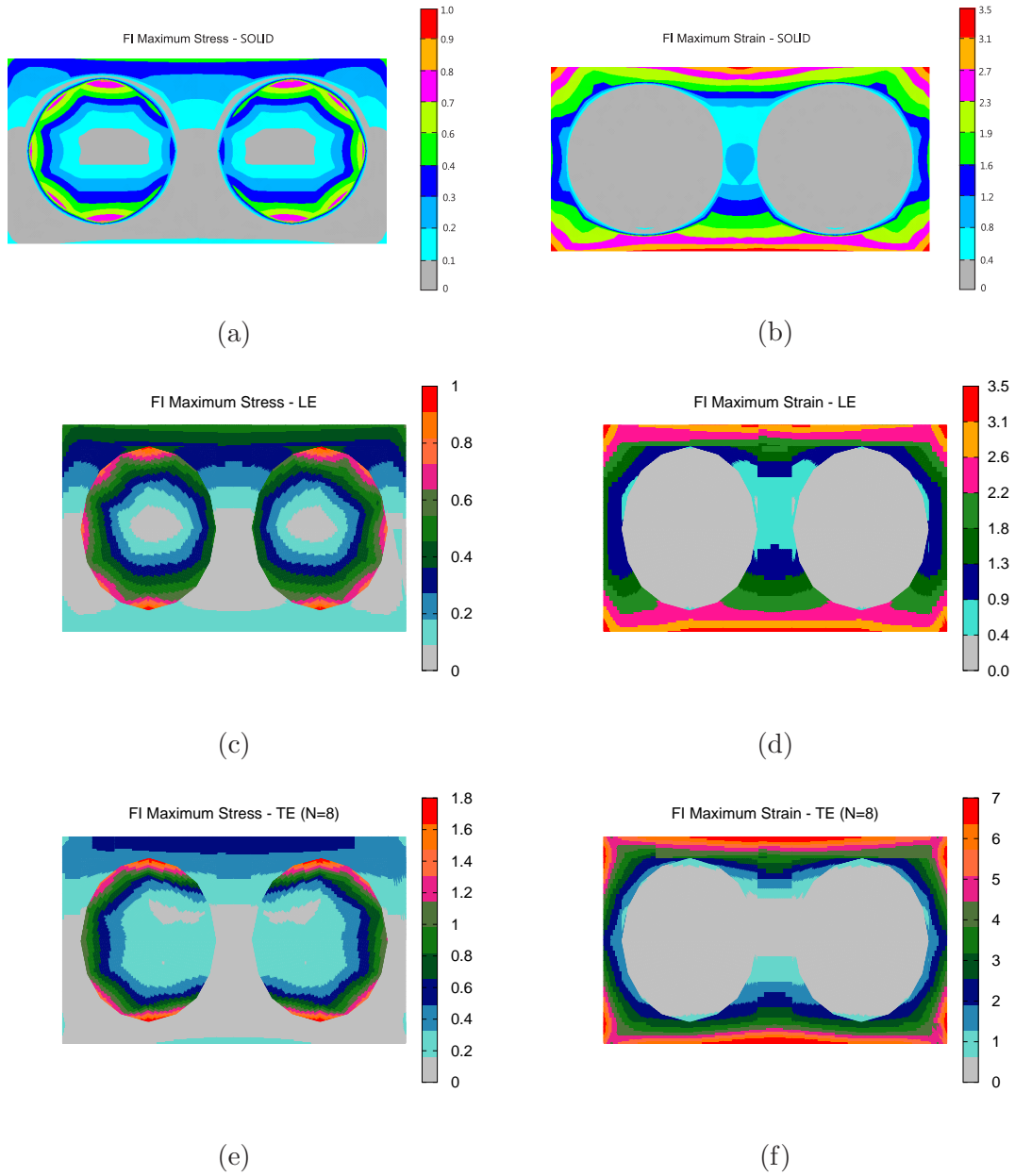
Figure 6.10.   Failure Indexes CW double cell models at $y = 0$.
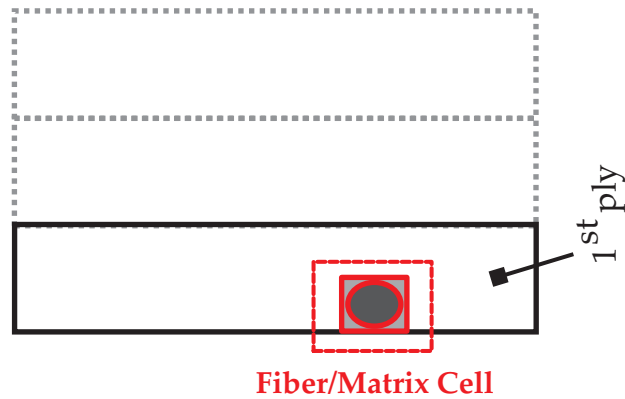
Figure 6.11. Three layers laminate with a fiber/matrix cell inclusion in the first ply.
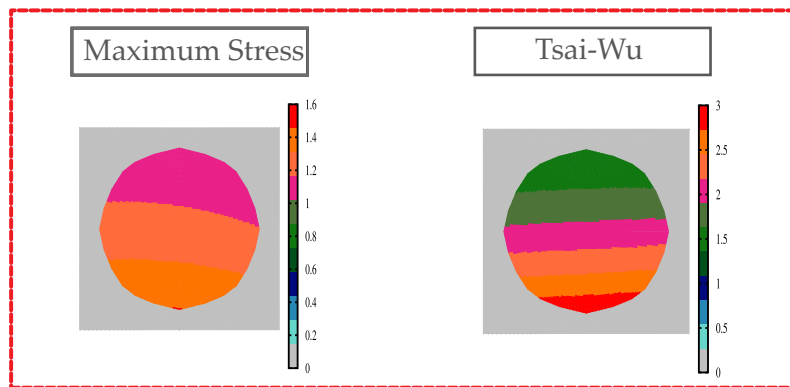
Figure 6.12. Maximum stress and Tsai-Wu criteria FI distributions in the cell subdomain in the 1st ply of the three layers laminate. Bending load applied.
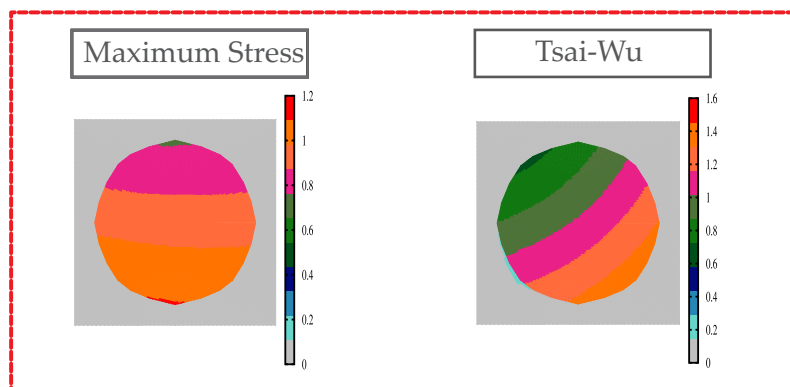
Figure 6.13. Maximum stress and Tsai-Wu criteria FI distributions in the cell subdomain in the 1st ply of the three layers laminate. Torsion load applied.
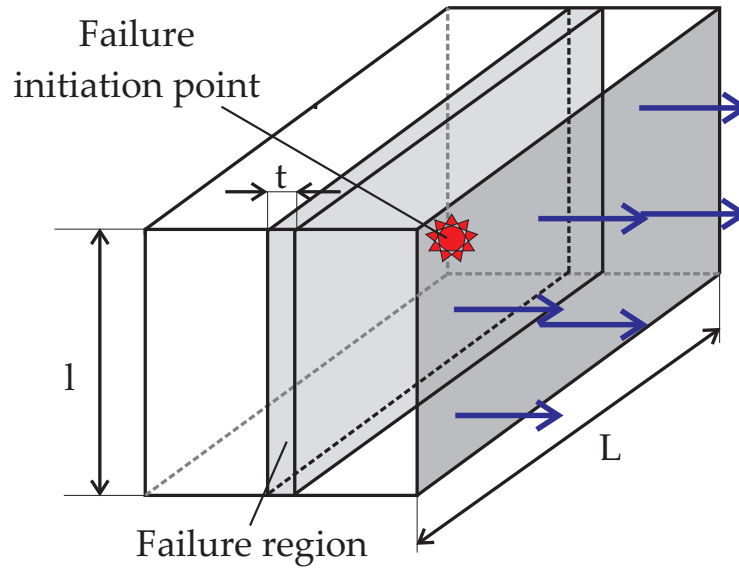
Figure 6.14.   Isotropic square cell for a mesh objectivity preliminary assessment.
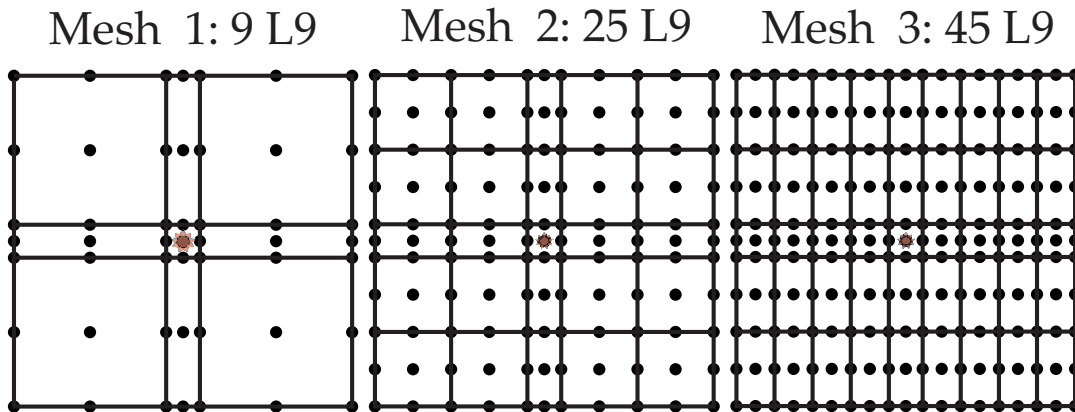
Figure 6.15.   Model descriptions for the mesh objectivity preliminary assessment: 9 L9, 25 L9, 45 L9.
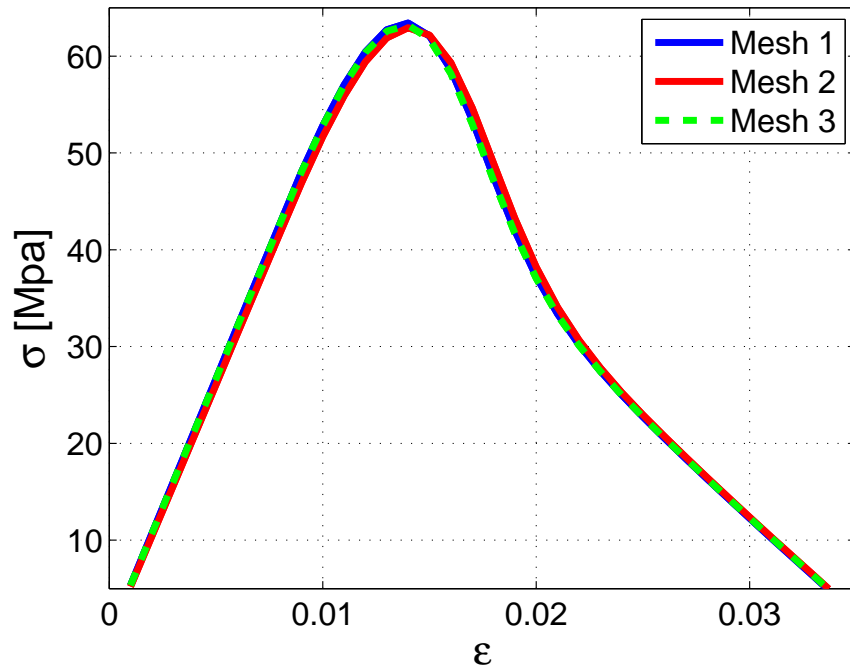
Figure 6.16. Stress/strain curve for the mesh objectivity preliminary assessment.
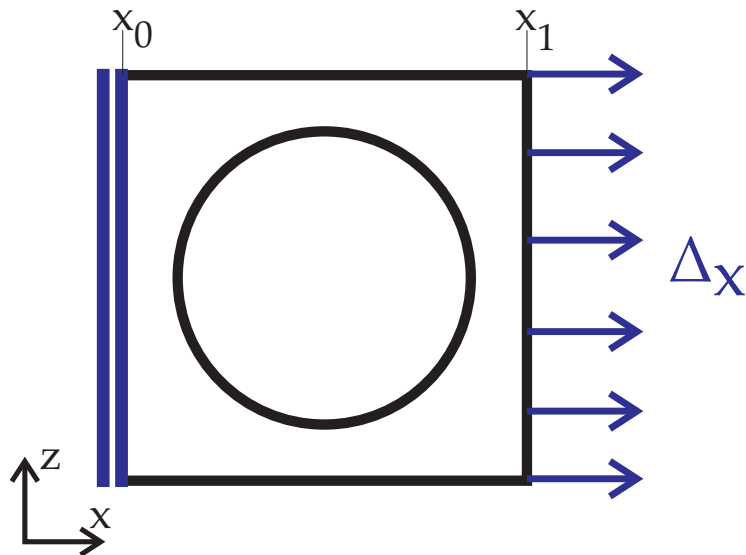

Figure 6.17. Single fiber RUC progressive failure analysis boundary conditions.
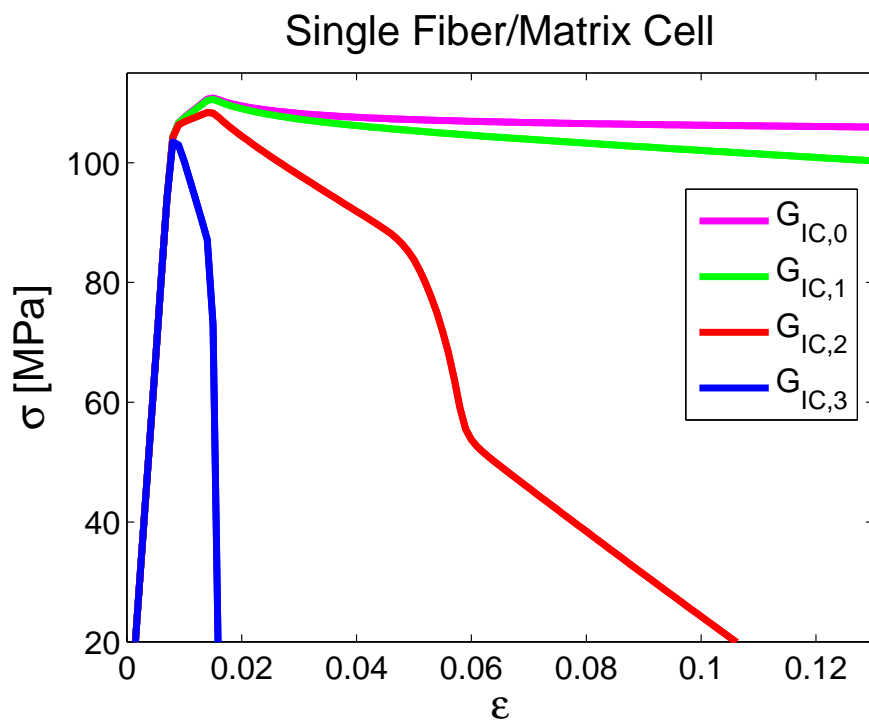
Figure 6.18. Stress/strain curve for the progressive failure of the single fiber RUC varying G_{IC}.

(a)

(a)

(b)

(b)

(c)

(c)
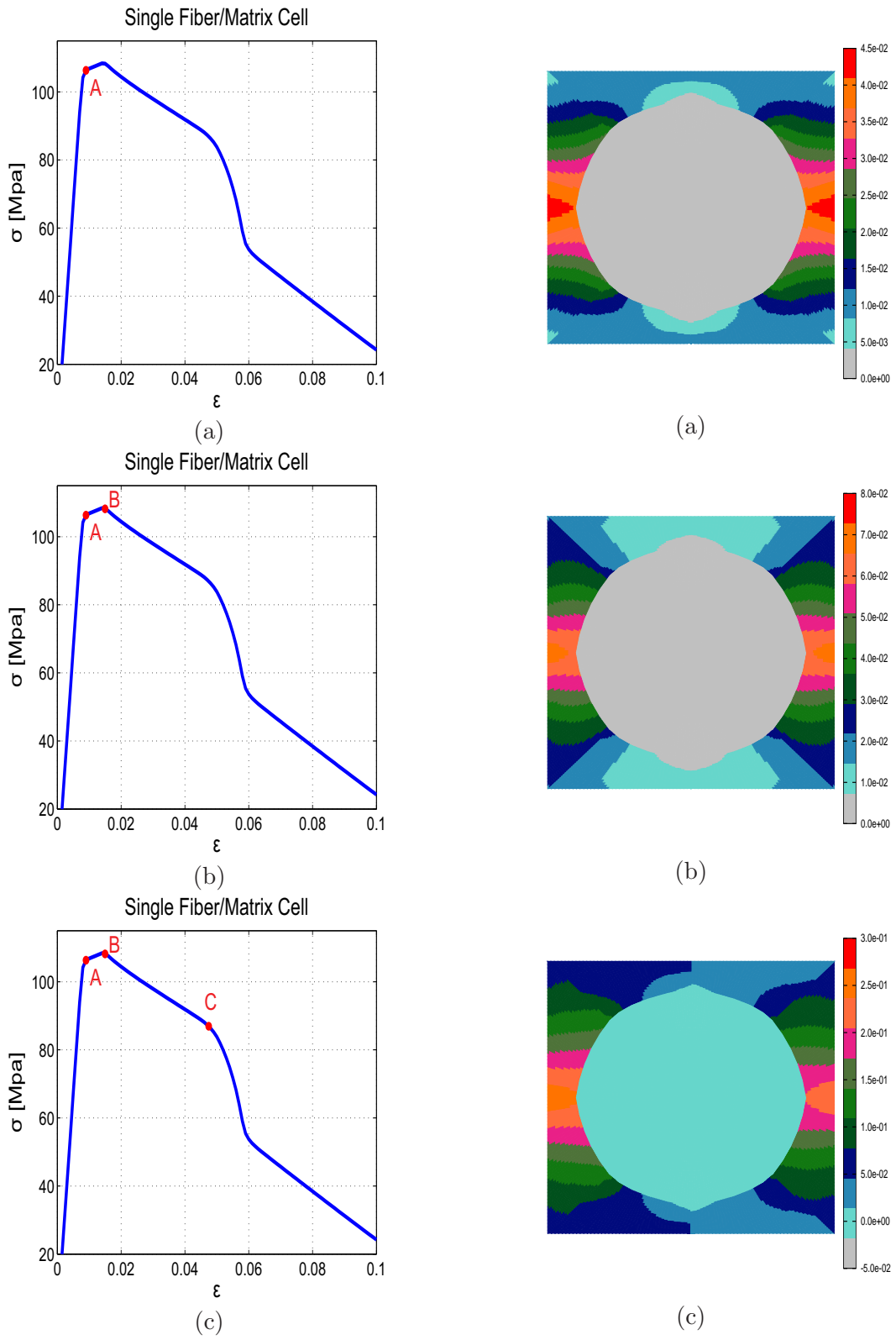
Figure 6.19.   Crack path for the single fiber RUC, $G_{IC,2}$ curve.

129